International Journal of Pharmaceutics 660 (2024) 124308

Contents lists available at ScienceDirect

International Journal of Pharmaceutics

journal homepage: www.elsevier.com/locate/ijpharm

Production of mono and bilayer devices for wound dressing by coupling of electrospinning and supercritical impregnation techniques

Stefania Mottola [a,c], Gianluca Viscusi [a,c], Raffaella Belvedere [b], Antonello Petrella [b,*], Iolanda De Marco [a,c,**], Giuliana Gorrasi [a,c]

[a] Department of Industrial Engineering, University of Salerno, Via Giovanni Paolo II, 132, 84084 Fisciano, Salerno, Italy
[b] Department of Pharmacy, University of Salerno, Via Giovanni Paolo II, 132, 84084 Fisciano, Salerno, Italy
[c] Research Centre for Biomaterials BIONAM, University of Salerno, Via Giovanni Paolo II, 132, 84084 Fisciano, Salerno, Italy

ARTICLE INFO

Keywords:
Electrospinning
Supercritical impregnation
Wound dressing
Drug release
Cytotoxicity

ABSTRACT

In this paper, electrospinning and supercritical impregnation were coupled to produce polyurethane fibrous membranes loaded with mesoglycan and lactoferrin. The proposed methodology allowed the production of three skin wound healing bilayer systems: a first system containing mesoglycan loaded through electrospinning and lactoferrin loaded by supercritical impregnation, a second system where the use of the two techniques was reversed, and a third sample where the drugs were both encapsulated through a one-step process. SEM analysis demonstrated the formation of microfibers with a homogeneous drug distribution. The highest loadings were 0.062 g/g for mesoglycan and 0.013 g/g for lactoferrin. Then, hydrophilicity and liquid retention analyses were carried out to evaluate the possibility of using the manufacturers as active patches. The kinetic profiles, obtained through *in vitro* tests conducted using a Franz diffusion cell, proved that the diffusion of the active drugs followed a double-step release before attaining the equilibrium after about 30 h. When the electrospun membranes were placed in contact with HUVEC, HaCaT, and BJ cell lines, as human endothelial cells, keratinocytes, and fibroblasts, respectively, no cytotoxic events were assessed. Finally, the capacity of the most promising system to promote the healing process was performed by carrying out scratch tests on HaCat cells.

1. Introduction

Traditional dressings were used in the past to treat wounds; they aimed to keep the wound dry and prevent the entry of harmful bacteria. Today, it is known that having a moist and warm environment around the wound allows for faster healing, as it favours the regeneration of cells and tissues (Field and Kerstein, 1994). Dressings can be distinguished based on their function (antibacterial, occlusive, debridement, absorbent), the material used, or the physical form in which they occur (ointment, film, foam, gel). A further classification can be made into traditional, modern, and advanced dressings (Boateng et al., 2008).

Traditional dressings (Rezvani Ghomi et al., 2019) require frequent substitutions to avoid the maceration of healthy tissues; moreover, they may have other disadvantages such as the adhesion due to excessive drainage.

Modern dressings were fabricated to improve the wound's healing function rather than simply covering and isolating it from the external environment. They are generally constituted by synthetic polymers and can be passive, interactive (Broussard and Powers, 2013; Gurtner et al., 2008) and bioactive (Rezvani Ghomi et al., 2019). Finally, advanced dressings refer to skin replacement through tissue engineering. Traditional and modern dressings are not in fact, able to replace lost tissue, facilitating wound healing. In this perspective, it is important to make an appropriate choice of the dressing to be used; this depends on the objective of the dressing, the condition of the wound, the level of activity, and the needs of patients /individuals. Therefore, the dressing should protect the wound from additional trauma, ensure environmental humidity, absorbe or removing excess exudate, prevente contamination and offer an environment favorable to the body's natural defense mechanisms (Korting et al., 2011).

In recent decades, several efforts have been made to find novel pharmacological approaches to wound care since almost all used treatment approaches are inadequate or ineffective. The use of topical bioactive drugs in lotions, creams, and ointments for targeted drug

* Corresponding author at: Department of Pharmacy, University of Salerno, via Giovanni Paolo II, 132, 84084 Fisciano, Salerno, Italy.
** Corresponding author at: Department of Industrial Engineering, University of Salerno, Via Giovanni Paolo II, 132, 84084 Fisciano, Salerno, Italy.
E-mail addresses: apetrella@unisa.it (A. Petrella), idemarco@unisa.it (I. De Marco).

https://doi.org/10.1016/j.ijpharm.2024.124308
Received 20 January 2024; Received in revised form 2 May 2024; Accepted 4 June 2024
Available online 6 June 2024

delivery is ineffective because the fluid is rapidly adsorbed. Transdermal patches are one of the most widely used approaches to local drug delivery. A transdermal patch is a patch or medicated adhesive film placed on the skin to provide, topically, a predefined dose of the active ingredient with a controlled release rate.

These advanced dressings are produced to ensure biological activity, while the loaded drugs are essential in wound healing.

Among the different polymeric support to produce modern wound dressing, electrospun fibers-based systems are gaining some interest from scientific community since they can be potentially used in different fields such as textiles, wound-dressing, filtration, sensor and drug-delivery, due to their unique properties (Çalamak et al., 2014; Di Salle et al., 2021; Viscusi et al., 2023c, Viscusi et al., 2023a; Viscusi et al., 2023b; Viscusi et al., 2021). The use of nanofiber membranes for wound healing applications has been investigated in recent years as an alternative to conventional devices. Electrospun fibers facilitate liquid evaporation as well as the prevention of bacterial contamination due to their pore structures and excellent oxygen permeability (Mistry et al., 2021; Wang et al., 2019). Moreover, drugs and other healing enhancers can be incorporated into nanofibers to improve the activity of these systems. A novel way to incorporate the active principle into the polymeric matrices concerns the use of the supercritical impregnation process (Darpentigny et al., 2020; Franco et al., 2019; Mottola et al., 2023) that ensures the impregnation of the drugs into the nanofibers enabling sustained drug release to promote the wound healing process (Calamak et al., 2015). Moreover, the process allows for combining the properties of different drugs. In the literature, many papers on the use of wound dressings were reported (Akduman et al., 2016; Chaushu et al., 2015; Franco et al., 2020; Kataria et al., 2014; R. et al., 2018; Saha et al., 2020; Yuan et al., 2021). All the systems described in these works have some active compounds that can improve the wound healing mechanism, but none of them have a combination of active compounds with different properties. By stating that this work is focused on the use of mesoglycan (MSG) and lactoferrin (LF) as very promising compounds that have a synergic effect in the wound healing process (Belvedere et al., 2021).

Regarding the choice of the type of wound dressing, there is still not the ideal polymer that could be suitable for all the stages of healing. However, it has been found that polyurethanes (PUs) are good candidates for application on skin lesions (Morales-González et al., 2022). They show good mechanical flexibility, biodegradability, and different physicochemical properties, making them suitable for obtaining fibers, coatings, and foams (Kasi et al., 2022). Moreover, their versatility is vast as well as their biocompatibility and biostability, properties appealing for application in the biomedical fields (Morales-Gonzalez et al., 2020).

In light of the above-reported statements, this work focused on the possibility of coupling two techniques (electrospinning and supercritical impregnation) in order to design a novel bilayer-based transdermal patch loading two active pharmaceutical compounds (MSG and LF) into PU fibres. Despite the wide use of the two methodologies in the biomedical/pharmaceutical fields, the combination of the two set processes opens the route to the exploration of innovative layered patches with tunable release kinetics and multipurpose features. The presence of two drugs with different intrinsic properties, allowed for exploiting their synergy, favouring the therapeutic effect and showing the potential to facilitate progression in applications of drug release modification and tissue engineering. Finally, it is possible to claim that this approach can be an appropriate choice for developing controlled-multi-release drug delivery systems.

2. Materials and methods

2.1. Materials

Polyurethane (PU) was purchased from Lubrizol, USA. N,N-Dimethylformamide (CAS: 68–12-2) and Tetrahydrofuran (CAS: 109–99-9) were acquired from Sigma Aldrich. Carbon dioxide (CO_2, purity 99 %) was supplied by Morlando Group S.R.L. (Sant'Antimo-NA, Italy). Sodium salt mesoglycan (MSG) was purchased from LDO (Laboratori Derivati Organici spa, Vercelli, Italy); it consists of heparin (40 % low molecular weight in the range 6.5–10.5 kDa and 60 % less than 12 kDa, sulphurylation degree 2.2–2.6), heparan sulfate (UFH-unfractionated heparin from 12 kDa up to 40 kDa; sulphurylation degree 2.6), and dermatan sulfate, deriving from epimerization of glucuronic acid of chondroitin sulfate (molecular weight 18–30 kDa, sulphurylation degree 1.3) with a total sulphurylation degree equal to 9.1. Lactoferrin from human milk (LF) was provided by Sigma Aldrich. Sodium hydroxide (CAS: 1310–73-2), hydrochloric acid solution 37 % v/v (CAS: 7647–01-0), urea (CAS: 57–13-6), lactic acid (CAS: 50–21-5) were purchased from Sigma Aldrich. Sodium chloride (CAS: 7647–14-5), trifluoroacetic acid (TFA) and Acetonitrile were purchased from Carlo Erba Reagents. Distilled water was produced using a lab scale distillation in our laboratory. Phosphate buffered saline solution (PBS, pH = 7.4) was prepared for the drug release study.

2.2. Supercritical impregnation plant

Fig. 1 depicts the sketch of a custom-made bench plant used for impregnation experiments. The plant's core is a high-pressure vessel made of stainless steel, with a volume of 100 mL, and sealed at both the top and bottom using two-finger clamps. To introduce carbon dioxide into the vessel, a diaphragm piston pump (Milton Roy, mod. Miltonroy B, Pont-Saint-Pierre, France) is employed, with the gas being cooled beforehand through a connected cooling bath. Mixing of the contents is facilitated by an impeller on the top cap, powered by an electric motor capable of adjusting its velocity. The pressure during operation is measured using a manometer (Parker, Minneapolis, MN, USA), while the temperature is monitored with a thermocouple with an accuracy of ± 0.1 °C. Electrically controlled thin bands, connected to a proportional–integral–derivative (PID) controller (Watlow, mod. 93, Toledo, OH, USA), are responsible for heating the vessel and maintaining it at a fixed temperature. At the end of the test, a micrometric valve (Hoke, mod. 1315G4Y, Spartanburg, SC, USA) is utilized for depressurization.

A tiny support, opened at the top and mounted axially on the impeller, is charged with an established quantity of MSG and LF. This quantity exceeds the drugs' solubility in CO_2 under the chosen pressure and temperature. A support containing a PU membrane was positioned at the bottom and covered with a paper filter. Finger-tight clamps are then closed, and CO_2 is pumped while the heating bands are switched on until the operating conditions are attained. Subsequently, the CO_2 supply is halted, the impeller is set in motion, and the system works in batch

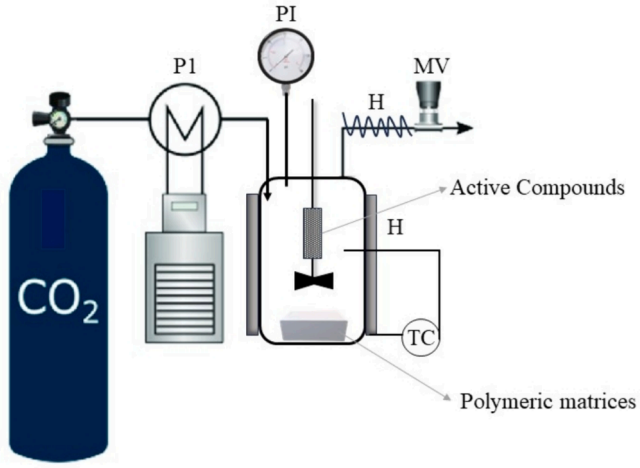

Fig. 1. Sketch of supercritical impregnation plant; P1 = CO_2 pump; PI = Pressure indicator. H = Heater; TC = thermocouple; MV = micrometric valve.

mode for the predetermined duration of the test. A slow depressurization process starts, maintaining a constant flow rate of 0.5 MPa/min. After attaining the atmospheric pressure, the loaded sample is retrieved and subjected to characterization. Each experiment was performed three times.

2.3. Electrospinning

Polymeric solutions for electrospun membranes were prepared as described from now on. Pure PU membrane was prepared as follows: polyurethane (20 % w/w) was dissolved in dimethylformamide/tetrahydrofuran solution (70/30 %v/v). PU + LF (after MSG impregnation on PU membrane) and PU + MSG (after LF impregnation on PU membrane) were obtained by dissolving the PU in the same above-reported solvent mixtures. Then 2 % w/w of the active compound (on a PU basis) was added to the solution. The produced systems will be labelled as PU/MSG@LF and PU/LF@MSG for the MSG-impregnated PU coated with a second electrospun layer loading LF and LF-impregnated PU with a second electrospun layer loading MSG. All solutions were stirred at T = 50 °C with a mixing rate of 320 rpm. Electrospinning parameters are hereinafter reported: voltage = 23.5 kV, flow rate = 1 mL/h, distance needle-collector = 23.5 cm, RH = 35 % and T = 25 °C. Climate-controlled electrospinning apparatus (EC-CLI, IME Technologies, Geldrop, The Netherlands) was used to produce fibrous membranes, setting a vertical setup.

2.4. Characterizations

To examine the morphology and identify elements, a scanning electron microscope (SEM) equipped with energy-dispersive X-ray spectroscopy analysis (Phenom ProX with EDS detector (Phenom-World BV, Netherlands)) was utilized. Before the analysis, a sputter deposited a thin layer of gold on the samples. Fiji software's Plot Profile plug-in was employed to extract plot profiles from SEM images, creating a bi-dimensional graph displaying pixel intensities within a selected area of 1000 μm^2. The x-axis represents the distance, while the y-axis represents the pixel's intensity. Lastly, the surface roughness parameter R_a, which is the arithmetic mean of the absolute values of profile height deviations from the mean line within the evaluation length, was calculated using equation (1):

$$Ra = \frac{1}{L}^{*} \int_0^L Z(x)dx \quad (1)$$

where Z(x) is the profile height function.

Liquid retention of electrospun fabric was performed by soaking for 24 h a pre-weighed mass of sample in 25 mL of different liquid solutions (PBS (pH = 7.4)), HCl solution (pH = 4), and sweat simulant (pH = 5.5)). Sweat simulant was prepared according to EN 1811:2011. After that, the samples were weighed again (M_{eq}). The retention degree was calculated through the equation (2):

$$Q, \% = \frac{M_0 - M_{eq}}{M_0} 100 \quad (2)$$

where M_0 is the initial weight of the samples.

Contact angle (CA) measurements of samples were performed using a high-resolution camera. Droplets of liquid (100 μL) were dispensed on a 1x1 cm^2 test sample at room temperature. Three contact angle measurements were recorded at different points for each specimen. The contact angle was determined through the Drop Analysis plugin by using Image J software.

The amount of impregnated MSG into the polymeric matrices was estimated by UV–vis spectrophotometry (model Cary 50, Varian, Palo Alto, CA, USA) (λ = 206 nm). The LF is quantified by HPLC analysis (Agilent). The analyzed sample is injected inside the column (Model Aeris WIDEPORE 3.6 μm XB-C18 ZORBAX ~ 300SB 3.5 μm C18), and pushed through the stationary phase by the mobile phase. The moving phases are prepared according to the literature (Yao et al., 2013): PHASE A = Aqueous phase containing 0.1 % TFA and PHASE B = organic phase containing acetonitrile/water/TFA (95:5:0.1).

The analysis time is 25 min, with a flow rate of 0.75 mL/min applying a gradient to the phases reducing the concentration of the A phase from 95 % to 25 % in 8 min, then returning to 95 % at 25 min (for phase B the concentration ranges from 5 % to 75 % in 8 min and then reduced again to 5 %). The LF identification wavelength is 270 nm.

Approximately 0.005 g of membrane was placed in 10 mL of PBS at 200 rpm and 37 °C. The loaded amounts of MSG and LF were evaluated when equilibrium is reached. The obtained absorbances were converted into active ingredient concentrations using a calibration curve. Release profile studies were performed at 37 °C using a static Franz diffusion cell 11 mL type C glass (Hosmotic SRL, Vico Equense, Naples, Italy) coupled with a UV/Vis spectrophotometer or HPLC for loading- analysis. The donor chamber and acceptor chamber were separated by a PVDF membrane with an outer diameter of 25 mm and a pore size of 0.45 μm. The receiving chamber was filled with PBS (pH = 7.4) at 37 °C with constant stirring (500 rpm). Aliquots of 200 μL were removed at specified intervals and replaced with an equal volume of fresh PBS.

2.5. Cell cultures

The HaCaT cell line (Human immortalized keratinocytes) was bought from CLS Cell Lines Service GmbH; BJ cells (Human immortalized fibroblasts) were purchased from American Type Culture Collection (ATCC® CRL2522™). The two cell lines were cultured as described in a previous paper (Belvedere et al., 2018). HUVEC cell line (Human Umbilical Vein Endothelial Cells) (ATCC PCS-100-010™) was cultured as reported in (Novizio et al., 2021) and kept in culture until passage 10. All the cells were grown at 37 °C in air-humidified 5 % CO_2.

2.6. Haemocytometer counting

PU fibers were treated by UV irradiation with a surface disinfection unit in a clean room for 60 min. Pieces of approximately 0.8 cm^2 were placed in the wells' growth medium, in which 2 x 10^5 fibroblasts/well and 1 x 10^5 keratinocytes/well were seeded the day before. An EVOS microscope (10x objective, Life Technologies Corporation) was used to take images after 24, 48, and 72 h. To confirm the obtained results, at each of the times previously reported, a haemocytometric count was performed after the detachment of the cells using trypsin and mixing equal volumes of cell suspension and 0.4 % trypan blue (Sigma-Aldrich) as reported in (Bizzarro et al., 2019). The Burker chamber with the trypan blue/cell mix was visualized thanks to an Axiovert 40 CFL optical microscope (Carl Zeiss MicroImaging GmbH). The number of viable cells per mL was evaluated by averaging the number of cells in one large square and multiplying the obtained value for $2x10^4$ (2 is a dilution factor).

2.7. In vitro wound healing assay

In a 24-well plastic plate, HaCaT cells were seeded (density of 1.5 × 10 5 per well). After 24 h at 100 % confluency, a wound was made in the cellular monolayer by gently scraping the cells with a sterile plastic p10 pipette tip. All experimental points were further treated with mitomycin C (10 μg/ml, Sigma-Aldrich; Saint Louis, MO, USA) to ensure the block of mitosis. Pieces of approximately 0.8 cm 2 were placed in the wells' growth medium for the time of the assay. The assay and the following analysis were performed as previously reported (Belvedere et al., 2017) The wounded cells were photographed at time 0 and 24 h by using Axiovert 5 microscope with Axiocam 208 color (Carl Zeiss; Oberkochen, Germany). A 5 × phase contrast objective was used. The migration rate was determined by measuring the difference in the distances covered by each wound edge from the initial time to the selected time points.

3. Results and discussion

3.1. Supercritical CO_2 impregnation of active principles

Starting from previous work, the operative conditions for the supercritical impregnation of the two active compounds were optimized to obtain the right amount necessary for the therapeutic range and to maintain the initial flexibility given potential industrial application (Mottola et al., 2023).

In the previous paper, the operative conditions employed were T = 50 °C and P = 150 bar. The amount of lactoferrin impregnated into the polymeric matrices was very low using these conditions. Experimental data reported in the literature (García-Casas et al., 2019) revealed that the solubilities of the active compounds increase by increasing the pressure, so a more significant amount of impregnated drug could be achieved by fixing the operative pressure at 200 bar and temperature equal to 40 °C. Starting from the impregnation kinetics performed in the previous work (Mottola et al., 2023), it was observed that the maximum loading was achieved for a contact time equal to 24 h both for MSG and LF; for these reasons, the time of contact for each test was set at 24 h. The depressurization rate affected the structure's flexibility, so it is preferable to slowly decrease the pressure to limit the stiffening of the polymer chains and ensure a certain flexibility. The depressurization was carried out at 5 bar/min for the above-reported reasons.

The obtained samples by coupling supercritical impregnation and electrospinning process are described below:

- PU/MSG + LF for both MSG and LF impregnated by supercritical process;
- PU/MSG@LF for the MSG-impregnated PU coated with a second electrospun layer loading LF;
- PU/LF@MSG for the LF-impregnated PU coated with a second electrospun layer loading MSG.

3.2. Characterization of the samples

3.2.1. Morphological characterization

Electrospun fibers were characterized in terms of morphological properties (Fig. 2).

The SEM images of the PU, shown in Fig. 2a, show a highly porous membrane structure made up of randomly oriented fibers. From the distribution of fiber diameters, it is possible to measure an average diameter of 1.58 ± 0.02 μm. The membrane diameters are not in the nanometric range, but considering the specific application, smooth nanofibers without beads are more important than the attainment of nanometric fibers (Viscusi et al., 2023c) As can be seen in Fig. 2b, the impregnation of the mesoglycan with subsequent electrospinning of lactoferrin does not generate substantial variations in the mean fibers' dimensions that are oriented in a random network but show a smaller mean diameter equal to 1.22 ± 0.03 μm. Besides, the sample PU/LF@MSG in Fig. 2c does not show any noticeable difference or modification in terms of fiber morphology, which preserves the average diameter of the pure PU sample. The SEM image shows that neither the film's porosity nor the fibers' orientation results were significantly modified. Fig. 2d reports the SEM image and fiber diameter distribution of PU/MSG + LF. Some crystals on the surface are present; they are attributable to the powder of the drugs. Also in this case, it is possible to verify that the impregnation of the active molecules does not constitute a problem for the morphology of the fibers, which remains quite unchanged. Finally, it is possible to state that the adopted methodologies do not alter the morphology and the dimensions of the fibers, making their use in wound healing applications still possible.

For example, Fig. 3 reports the EDX maps of the sample PU/MSG + LF.

The presence of the drugs on the membrane's surface is visible in the SEM image, and it is confirmed by the EDX maps, which also show the homogeneous distribution of sulfur (S) and iron (Fe), which are elements representative of the structure of mesoglycan and lactoferrin. Then, the profile plots (intensity vs. distance) of the SEM images were obtained

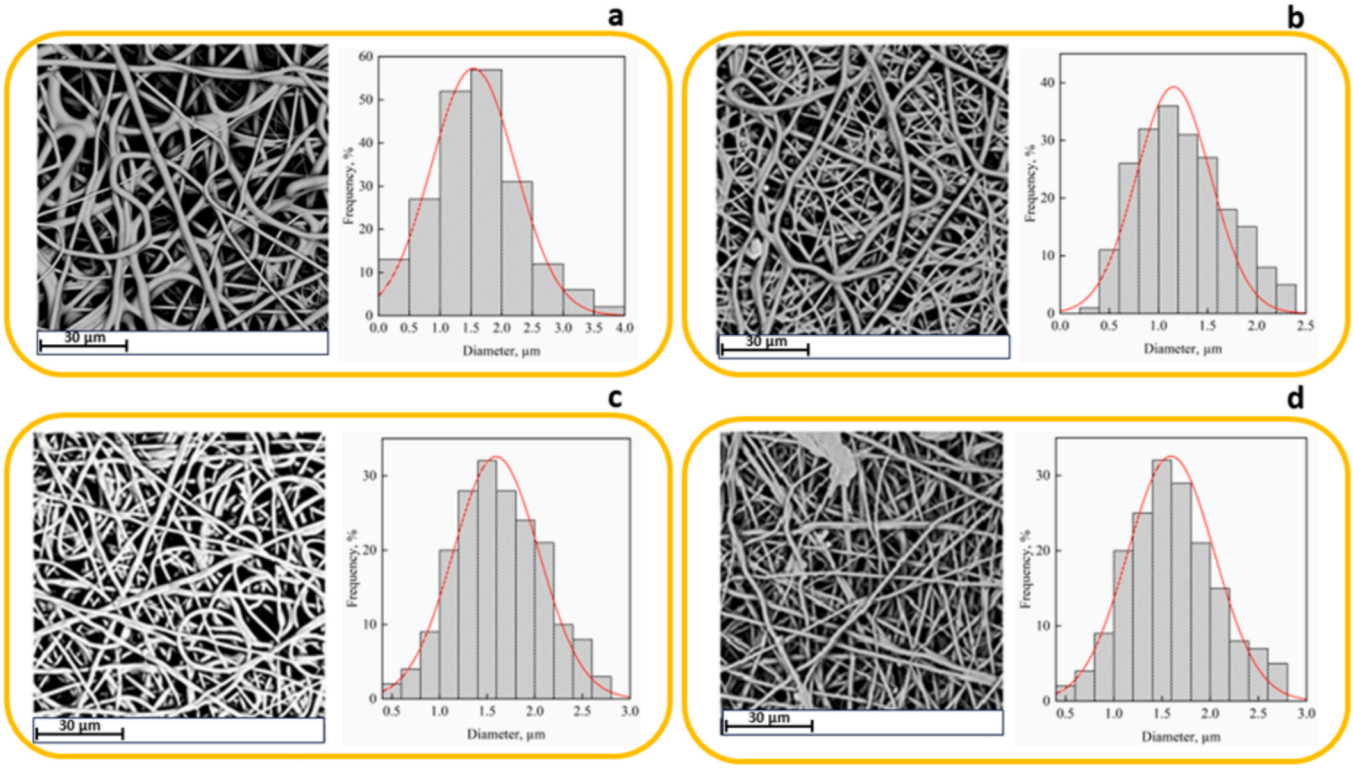

Fig. 2. SEM images and fiber's diameter distributions of a) PU; b) PU/MSG@LF; c) PU/LF@MSG and d) PU/MSG + LF.

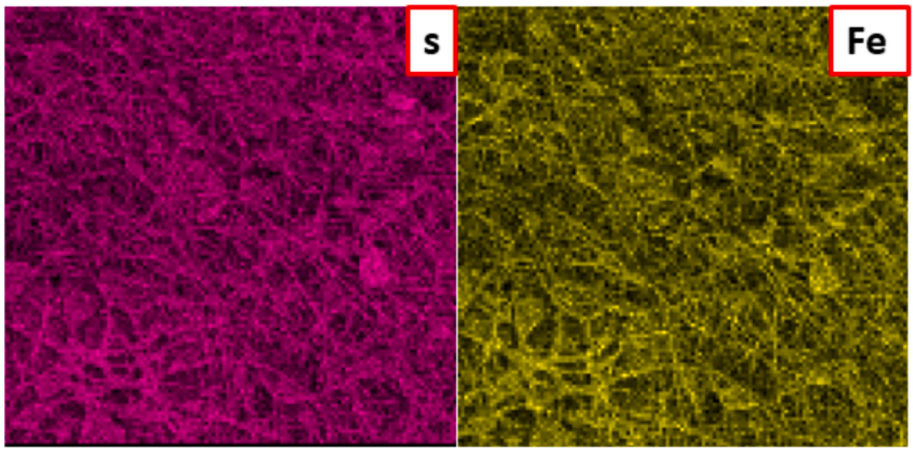

Fig. 3. EDX maps of PU/MSG + LF.

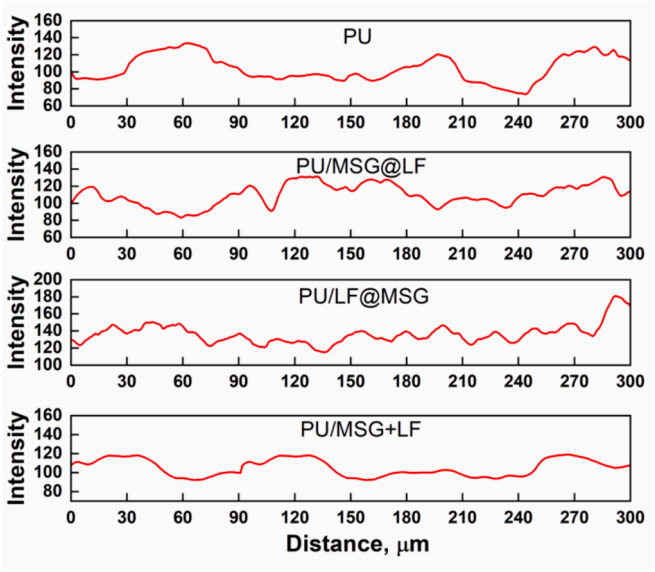

Fig. 4. Profile plots of PU electrospun systems.

(Fig. 4).

As evidenced from Fig. 4, the topographies slightly differ in height. Indeed, after the double process, the surface properties can change and affect the surface roughness of fibers. Some differences in profile height after loading MSG and LF were observed compared to neat PU. The R_a values are 97, 135, 109, and 199 for PU, PU/MSG@LF, PU/LF@MSG, and PU/MSG + LF, respectively. So, the impregnation of MSG and LF increases the surface roughness that is a fundamental parameter for cell differential and proliferation (Chen et al., 2017).

3.2.2. *Active principle loading*

The effective amount of drug impregnated or loaded directly into the PU fiber was calculated by UV/vis spectrophotometry in the case of MSG and by HPLC analysis in the case of lactoferrin, as previously described. Loading percentages are reported in the histogram shown in Fig. 5.

The loading values of all the samples are reported in Table 1.

The loading percentage obtained in this work agrees with the new operative conditions (Mottola et al., 2023); in particular, the use of a higher pressure allows to obtain a more significant impregnation percentage of lactoferrin, which is the compound desired in higher quantity. The higher loading is obtained for the device PU/LF@MSG where the mesoglycan was directly electrospun inside the fiber, whereas the supercritical impregnation process impregnates the lactoferrin; this combination allows to obtain the more significant loading because of the better disposition of the drug molecules inside and between the fibers.

3.2.3. *Retention of liquids tests*

Fig. 6 shows the retention degree (Q, %) of electrospun samples.

The trend of the retention capacity of the tested liquids is a function of various phenomena such as the surface roughness, the degree of porosity, the weak interactions involving the surface groups, and the surface charge properties. Regarding PBS (pH = 7.4), PU has a higher absorption capacity (125 %) because of its porous structure. At pH = 7.4, the high degree of absorption of the sample could be ascribed to the porosity of the membranes. The presence of the MSG and LF determines slight variations in terms of absorption (92 % for MSG and 74 % for LF), probably attributable to the molecular hindrance of the drugs. This effect is considerably more evident in the case of the double impregnation system (34 %), which could have caused a reduced free volume and a thickened polymer fiber. The sweat simulant has a pH = 5.5, close to the point of zero charge of the PU membrane, implying that the total positive charge equals the negative one. Therefore, the membrane possesses a zero net charge, and the water entry is overall because of the diffusion into the polymer network. However, the trend observed for the pH = 7.4 system is confirmed. Lactoferrin could contribute more to the reduction of the retention degree (58 %) since it is a protein naturally present in biological liquids (tears and sweat) that may be released from the fibers more quickly in the presence of salts. So, the LF could diffuse towards the liquid medium, leading to pore generation, which could improve water absorption. This trend was also observed in acidic conditions (pH = 4). The double-layer system shows no statistically noticeable variations in absorption, while the double-impregnation system shows a reduction of 66 %. Below the isoelectric point, the H^+ ions favor the protonation of the groups onto the surface. The free volume increases due to the presence of positive charges on the surface of the fibers, which repel each other electrostatically.

3.2.4. *Contact angle*

The membranes produced can potentially be used for biomedical applications. Since the skin is exposed to the external environment and, therefore, to possible contact with water, a preliminary study on the system's degree of hydrophilicity/hydrophobicity is appropriate. Wettability is a crucial factor in biocompatibility (Joshi et al., 2015). For each sample, contact angle measurements were carried out every 5 s. Fig. 7 shows the trend of the contact angles over time.

The pristine PU electrospun membrane possesses CA≃ 100°, as demonstrated in a previous work (Mottola et al., 2023) This value is an indicator of the fact that the drops have difficulty diffusing to the surface due to the hydrophobicity of the non-woven structure of the membrane.

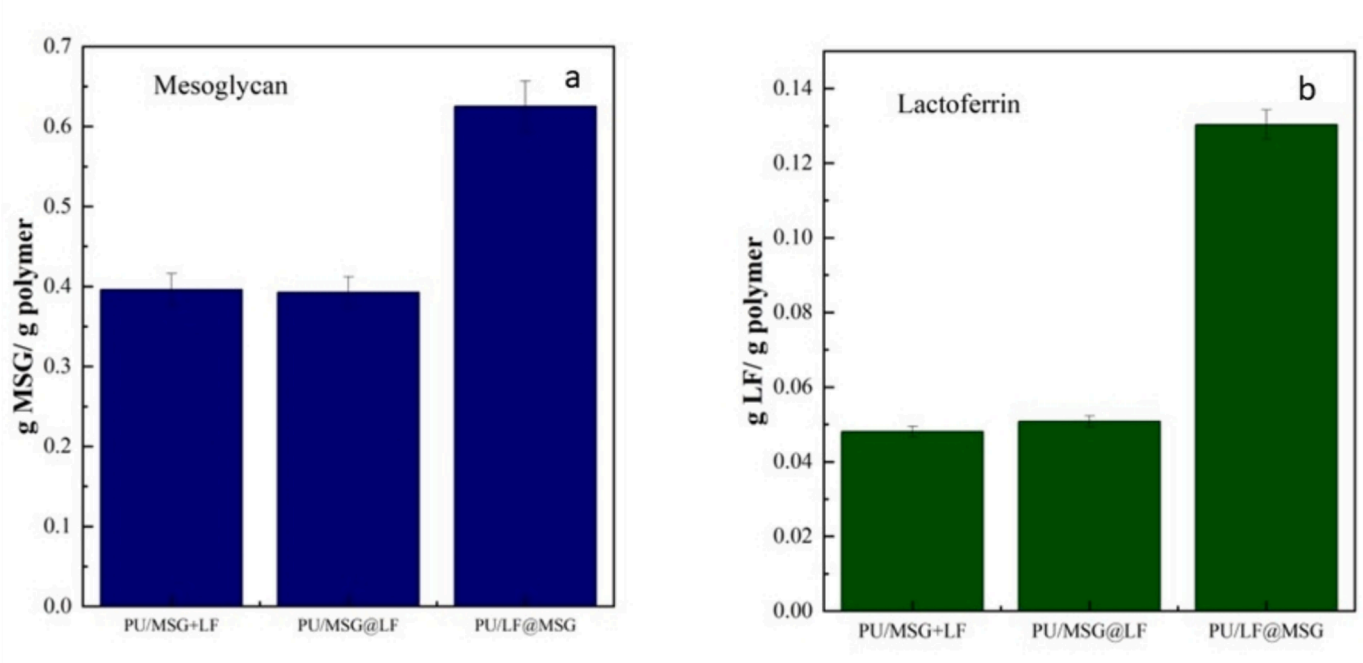

Fig. 5. Loading of the two active principles on the different devices (a) mesoglycan (b) lactoferrin.

Table 1
Loading values of electrospun membranes.

Sample	Active principles	Loading $g/g_{polymer}$
PU/MSG + LF	MSG	0.039
	LF	0.048
PU/MSG@LF	MSG	0.039
	LF	0.050
PU/LG@MSG	MSG	0.062
	LF	0.013

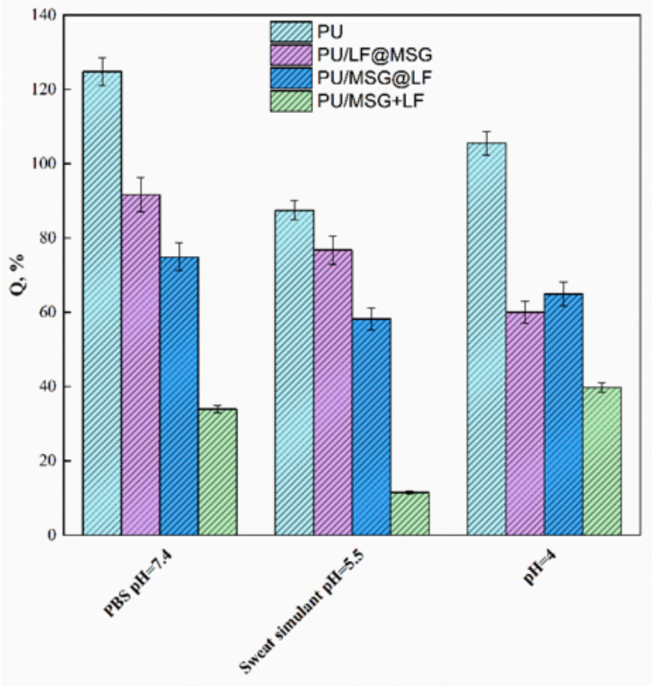

Fig. 6. Retention degree values of PU membranes.

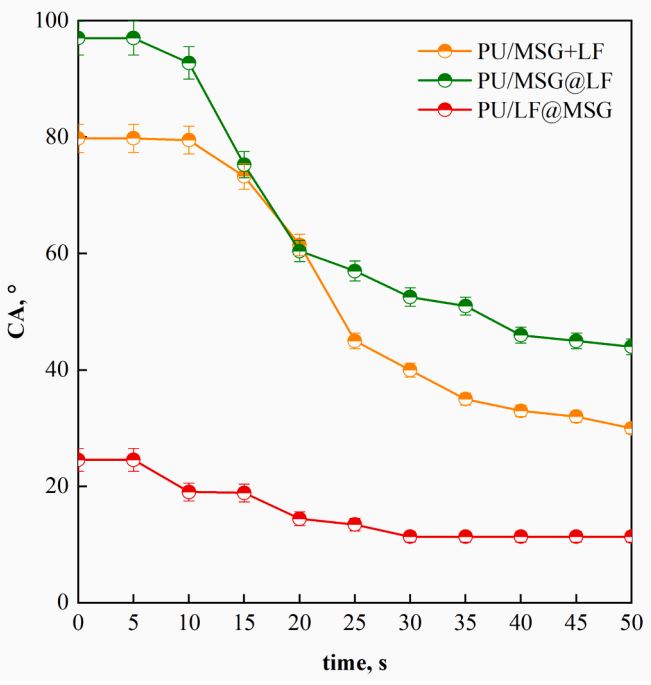

Fig. 7. Trends of water contact angle for the different specimens.

The test shows that the PU/MSG@LF sample is highly hydrophobic (initial CA = 97°), which could be due to an increase in the roughness of the fiber and a reduction in the active sites due to the interaction between it and the group functionalities of polyurethane. The presence of LF into PU/LF@MSG, instead, induces an increase in the degree of hydrophilicity (CA = 80°) since, given its chemical structure, intercalation within the fibers is favored with an intensification in the free volume between the pores and a reduction in roughness which might form spaces among the random fibers, keeping the fibers apart. However, the sample with double impregnation shows an intermediate behavior (CA

= 24°) between the two single systems. After about 30 s, the CA reached an equilibrium state that does not change over time. In particular, the steady-state values are 44°, 11°, and 30° for PU/MSG@LF, PU/LF@MSG, and PU/MSG + LF, respectively. In this context, the best system appears to be the PU/MSG@LF, which has a greater contact angle. This aspect allows adsorption by external liquids such as water to be limited, thus allowing the stability of the patch to be preserved.

3.2.5. Release kinetic profiles of MSG and LF

Release tests were carried out using a Franz diffusion cell. Fig. 8 reports LF (a) and MSG (b) release profiles.

In Fig. 8a, the LF release profiles are reported. The PU/LF@MSG sample showed that LF was released with a slow and controlled kinetic. 50 % of LF was released after 5.4 h and 3.4 h, for LF and MSG, respectively; this is a symptom that some molecules are present on the surface. Besides, the residual amount inside the PU membrane was released with a slower kinetic. The equilibrium stage was reached in 31 and 33 h for LF and MSG, respectively. Focusing on the sample PU/MSG@LF, it can be noted that 50 % of LF and MSG were released in 30 min before attaining equilibrium after about 30 h. The faster release of LF in PU/MSG@LF compared to PU/LF@MSG can be due to the impregnation process, which allowed LF to stack onto the PU fibers, enabling the release to be faster since the diffusion of the molecules from the surface to the liquid bulk was favored.

Regarding MSG, its faster release in PU/MSG@LF can be due to the opening of the polymeric network after contacting with CO_2 due to the impregnation of LF, which could favor the increase in pore size and free volume. In the case of the double impregnation sample, it was possible to observe a burst effect of around 15 % after 1.4 h for LF and 50 % after 2.5 h for MSG. The 50 % of LF and MSG were released in 4.30 h and 2.7 h, respectively. Finally, the equilibrium regime was reached after 32 h for both systems. The first step concerns the released drug present on the surface while, in the second phase, the drug incorporated into the polymer matrix was released. LF can be quickly released for shorter times, while MSG releases for longer times. The lower sterical hindrance, the better compatibility with PU fibers, and the smaller pore size could be responsible for the delayed release of MSG. The liquid must diffuse into the polymer, solubilize the MSG, and diffuse again towards the external medium, explaining why the release can be significantly prolonged. This could be considered an advantage for the topical release of drugs for wound healing applications, allowing the operation of the patch for longer times. The release data mathematical modeling was carried out by applying the statistical Weibull model (equation (3) (Romero et al., 1989; Weibull, 1951):

$$\frac{M}{M_0} = 1 - exp^{-\frac{1}{A_1} * t^{b_1}} \tag{3}$$

where M = drug dissolved as a function of time t, M_0 = equilibrium released amount of drug, A = scale factor and b = parameter related to the drug release mechanism (Mircioiu et al., 2019). In this work, the Weibull model was modified (equation (4) by introducing the parameter t_m as the time corresponding to the maximum cumulative drug release of the first phase (diffusion phase):

$$\frac{M}{M_0} = \theta\left(1 - exp^{-\frac{1}{A_1} * t^{b_1}}\right) + (1-\theta) * \left(1 - exp^{-\frac{1}{A_2} * (t - t_m)^{b_2}}\right) \tag{4}$$

where θ represents the contribution of the diffusion-controlled mechanism, while the second one (1-θ) concerns the contribution of the polymeric chain relaxation. The Weibull's model parameters are reported in Table 2.

The release of a compound should be analyzed by considering a series of phenomena and factors, such as the drug's properties, the polymer's structural characteristics, the release environment, and interactions (Fu and Kao, 2010). The PU/MSG + LF sample shows a θ = 0.43 and 0.21 for MSG and LF, respectively. The lower θ in the case of LF could be due to the difficulty for LF to diffuse, caused by the high hindrance of the molecules, which could limit its movement through the fibrous network. Besides, the impregnation favored the slower diffusion of both drugs since the lower θ parameters (0.75 and 0.8 for MSG in PU/MSG@LF and PU/LF@MSG, respectively, and 0.33 and 0.48 for LF in

Table 2
Kinetic parameters evaluated from the fitting process of release data using equation (4).

	sample	A_1	A_2	b_1	b_2	t_m	θ	R^2
MSG	PU/LF@MSG	3.04	88.9	0.94	3.28	0.95	0.8	0.984
	PU/MSG@LF	0.68	56.2	0.33	4.59	0.42	0.75	0.958
	PU/MSG + LF	2.73	2.2	0.55	1.16	0.98	0.43	0.986
LF	PU/LF@MSG	1.39	13.1	0.52	1.07	1.21	0.33	0.975
	PU/MSG@LF	0.48	1.5	0.42	0.46	0.50	0.48	0.995
	PU/MSG + LF	32.3	1.2	1.91	0.73	0.38	0.21	0.975

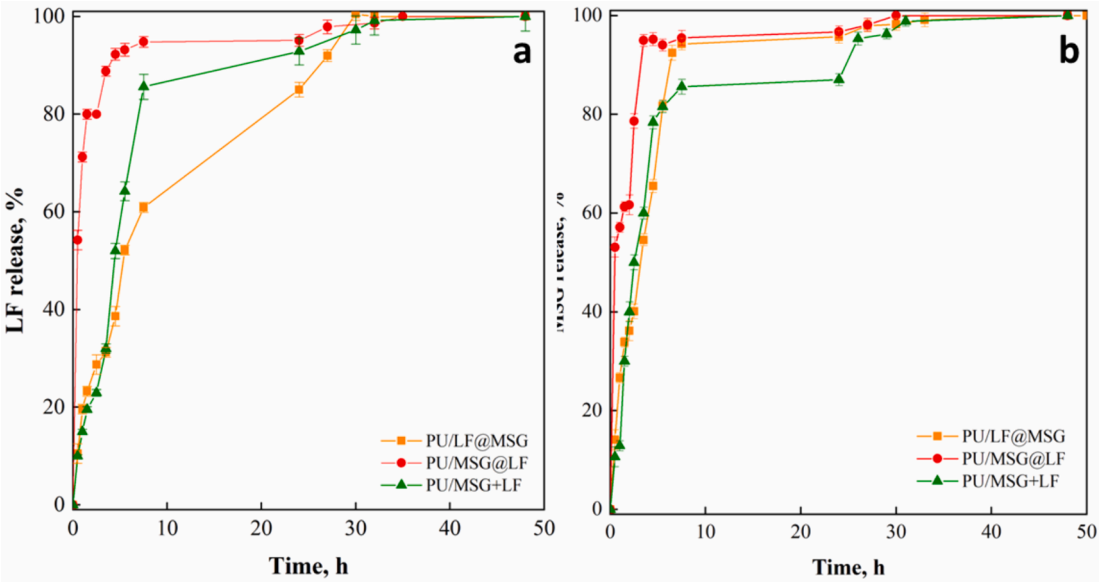

Fig. 8. Release profiles of a) LF and b) MSG from the PU based membranes.

PU/LF@MSG and PU/MSG@LF, respectively). The ratio $1/A_1$ and $1/A_2$ could be studied as the kinetic constants of the diffusion and relaxation phenomena. For MSG, the diffusion constant of PU/MSG@LF is higher than the relaxation one. Besides, both are higher than the values $1/A_1$ and $1/A_2$ for PU/LF@MSG. For the sample PU/MSG + LF, the diffusion and the relation phenomena appeared to occur in parallel, while the $1/A_1$ and $1/A_2$ showed to be quite similar, as evidenced by the θ values close to 50 %. For LF, the diffusion constant of PU/MSG@LF is higher than the relaxation one. Besides, both are higher than the values $1/A_1$ and $1/A_2$ for PU/LF@MSG. The lower value of $1/A_2$ for this latter sample proved the faster diffusion of LF when it is loaded inside the fibers. The values of b_1 and b_2 further prove the reported statements. For the sample PU/MSG + LF, the diffusion of LF is negligible compared to the relaxation since the 1/A1 value is quite low. All the systems showed a double-step release mechanism with a $t_m \neq 0$.

3.3. Cytotoxicity tests

All the polyurethane samples have been tested on HUVEC, HaCaT, and BJ cells as described in (Mottola et al., 2023). Fig. 9 reports the results obtained through the hemocytometer count after 24, 48, and 72 h from placing the three different patches in contact with the cells. At each experimental time, the levels of the number of treated cells remained very similar to the not-treated ones. The absence of notable differences suggests that no *in vitro* toxic events are registered in the presence of all samples.

Considering the encouraging results obtained about the absence of toxic effects of the PU patches, we have selected the one that had shown the best characteristics to prove its efficacy on cell motility. As a preliminary investigation, we used the HaCaT cells on which we also tested

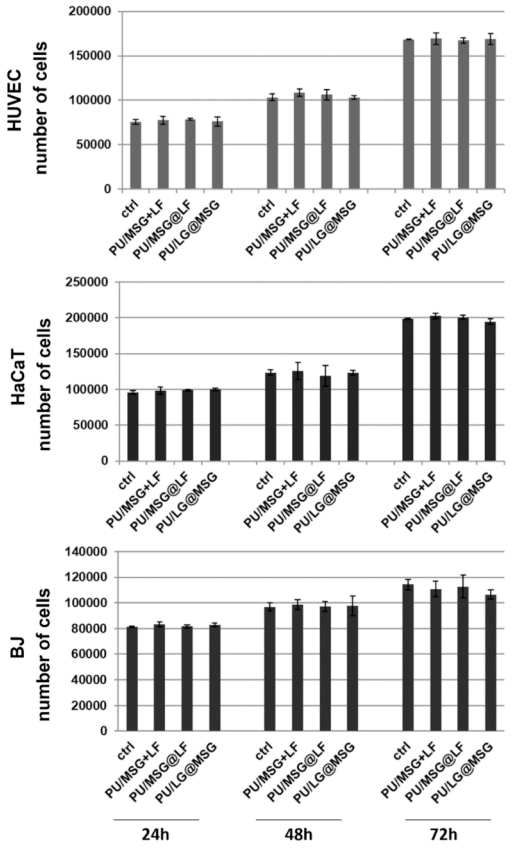

Fig. 9. Hemocytometer counts of HUVEC, HaCaT and BJ cells at 24, 48, and 72 h of contact with PU/MSG + LF, PU/MSG@LF and PU/LF@MSG. The data represent the mean of three experiments performed in triplicate with similar results.

the cell medium containing the active substances, mesoglycan and lactoferrin, released after 30 h by using Franz's cell as described in the materials and methods section. Thus, after becoming confluent, keratinocytes were gently injured with a sterile plastic tip to create a scratch that could heal by migration toward the scratched area. The wounds were imaged immediately afterwards the scratch formation and after 24 h of incubation.

As reported in Fig. 10, in the presence of PU/LF@MSG and of medium released from PU/LF@MSG, HaCaT cells acquired a significant migration speed to move towards the scratch areas after 24 h of treatment. Interestingly, no differences have been revealed between the two experimental points when compared to non-treated cells. Overall, the obtained results first confirmed the positive influence of mesoglycan and lactoferrin on cell motility and highlighted the appealing very similar effect of the TPU projected as previously described. These findings reinforce the concept of the potential use of a device structured with PU containing mesoglycan and lactoferrin for tissue regeneration in skin wound healing.

4. Conclusions

Mono and bilayer PU membranes charged with MSG and LF were produced by coupling electrospinning and supercritical CO_2-assisted impregnation for wound dressing application. The three devices were produced, combining the two techniques in different ways. The supercritical impregnation tests were carried out using the following operating conditions: P = 200 bar and T = 40 °C. The SEM analysis of the samples showed that the selected process conditions did not change the fibers. Indeed, they keep the initial size and orientation. The results report the loading of the two active ingredients following 24 h of processing: an MSG loading of 6.2 % is obtained in the case of the sample with electrospun MSG.

In comparison, the amount of lactoferrin impregnated reaches about 1.3 % in the sample with MSG electrospun, which proves to be the most promising sample for the loading percentages reached. Release tests demonstrated the benefits of fiber impregnation; in fact, the comparison of the three samples showed that the sample with MSG electrospun allows a slower and more homogeneous release, unlike the other two samples; in all cases, a release time of about 28–30 h for mesoglycan and about 25 h for lactoferrin was found. Cytotoxicity assays were performed to evaluate the effects of the system on fibroblasts, endothelial cells, and keratinocytes. Besides, the performance of PU/LF@MSG on favoring the healing process was demonstrated by carrying out scratch tests on HaCaT cells. The compatibility of these polyurethane fibers with cell viability makes them promising for application in the field of interest. As a result of the various characterizations, it can be concluded that the processes implemented are functional for the realization of patches suitable for skin wound healing.

CRediT authorship contribution statement

Stefania Mottola: Writing – original draft, Validation, Software, Methodology, Investigation, Formal analysis, Data curation. **Gianluca Viscusi:** Writing – original draft, Validation, Software, Methodology, Investigation, Formal analysis, Data curation. **Raffaella Belvedere:** Validation, Methodology, Investigation, Formal analysis, Data curation. **Antonello Petrella:** Supervision, Resources, Project administration, Conceptualization. **Iolanda De Marco:** Writing – review & editing, Supervision, Resources, Project administration, Conceptualization. **Giuliana Gorrasi:** Writing – review & editing, Supervision, Resources, Project administration, Conceptualization.

Declaration of competing interest

The authors declare that they have no known competing financial interests or personal relationships that could have appeared to influence

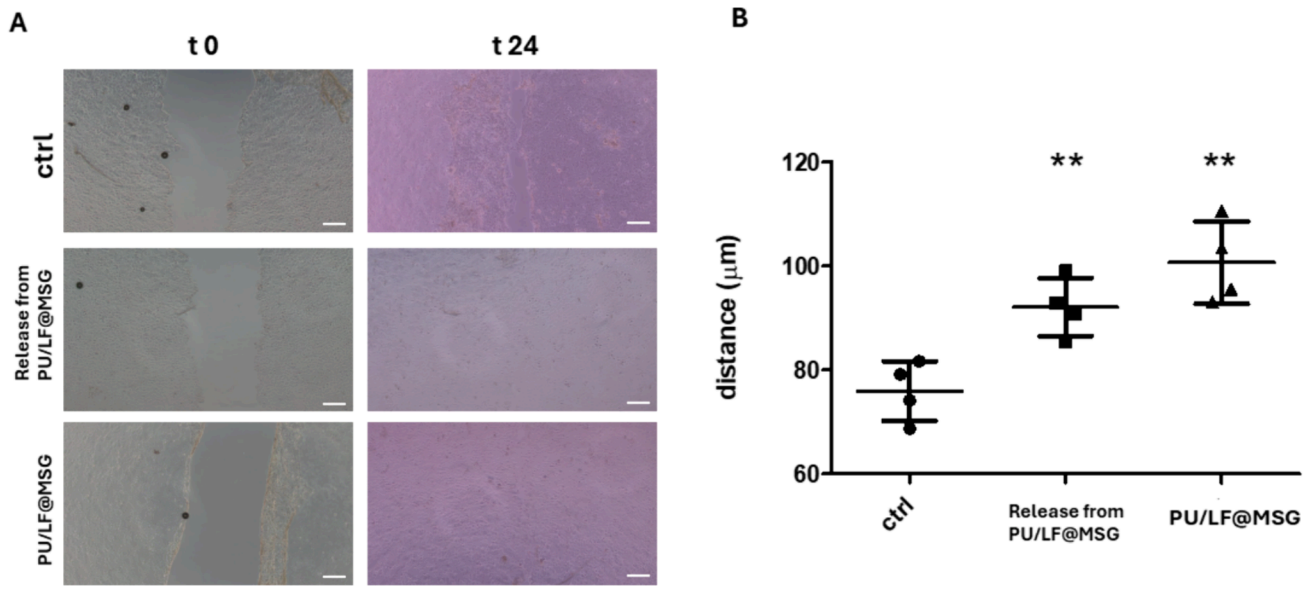

Fig. 10. A) Representative images of wound healing assay in HaCaT cells performed by using the medium containing mesoglycan and lactoferrin released from the_PU/LF@MSG and the PU/LF@MSG directly added to wells as reported in Material and methods section B) Results from the analysis of the migration assay. The data represent the mean of n = 4 independent experiments ± SD; significant differences from control conditions are indicated by asterisks (**p ≤ 0.01).

the work reported in this paper.

Data availability

No data was used for the research described in the article.

References

Akduman, C., Özgüney, I., Kumbasar, E.P.A., 2016. Preparation and characterization of naproxen-loaded electrospun thermoplastic polyurethane nanofibers as a drug delivery system. Mater. Sci. Eng. C 64, 383–390. https://doi.org/10.1016/J.MSEC.2016.04.005.

Belvedere, R., Bizzarro, V., Parente, L., Petrella, F., Petrella, A., 2017. The pharmaceutical device Prisma® skin promotes in vitro angiogenesis through endothelial to mesenchymal transition during skin wound healing. Int. J. Mol. Sci. 18, 1614. https://doi.org/10.3390/IJMS18081614.

Belvedere, R., Bizzarro, V., Parente, L., Petrella, F., Petrella, A., 2018. Effects of Prisma® Skin dermal regeneration device containing glycosaminoglycans on human keratinocytes and fibroblasts. Cell Adh. Migr. 12, 168–183. https://doi.org/10.1080/19336918.2017.1340137.

Belvedere, R., Pessolano, E., Novizio, N., Tosco, A., Eletto, D., Porta, A., Filippelli, A., Petrella, F., Petrella, A., 2021. The promising pro-healing role of the association of mesoglycan and lactoferrin on skin lesions. Eur. J. Pharm. Sci. 163 https://doi.org/10.1016/J.EJPS.2021.105886.

Bizzarro, V., Belvedere, R., Pessolano, E., Parente, L., Petrella, F., Perretti, M., Petrella, A., 2019. Mesoglycan induces keratinocyte activation by triggering syndecan-4 pathway and the formation of the annexin A1/S100A11 complex. J. Cell. Physiol. 234, 20174–20192. https://doi.org/10.1002/JCP.28618.

Boateng, J.S., Matthews, K.H., Stevens, H.N.E., Eccleston, G.M., 2008. Wound healing dressings and drug delivery systems: a review. J. Pharm. Sci. 97, 2892–2923. https://doi.org/10.1002/JPS.21210.

Broussard, K.C., Powers, J.G., 2013. Wound dressings: selecting the most appropriate type. Am. J. Clin. Dermatol. 14, 449–459. https://doi.org/10.1007/S40257-013-0046-4/FIGURES/2.

Calamak, S., Aksoy, E.A., Erdogdu, C., Sagıroglu, M., Ulubayram, K., 2015. Silver nanoparticle containing silk fibroin bionanotextiles. J. Nanopart. Res. 17, 1–9. https://doi.org/10.1007/S11051-015-2895-7/FIGURES/8.

Çalamak, S., Erdoğdu, C., Özalp, M., Ulubayram, K., 2014. Silk fibroin based antibacterial bionanotextiles as wound dressing materials. Mater. Sci. Eng. C 43, 11–20. https://doi.org/10.1016/J.MSEC.2014.07.001.

Chaushu, L., Weinreb, M., Beitlitum, I., Moses, O., Nemcovsky, C.E., 2015. Evaluation of a topical herbal patch for soft tissue wound healing: an animal study. J. Clin. Periodontol. 42, 288–293. https://doi.org/10.1111/JCPE.12372.

Chen, H., Huang, X., Zhang, M., Damanik, F., Baker, M.B., Leferink, A., Yuan, H., Truckenmüller, R., van Blitterswijk, C., Moroni, L., 2017. Tailoring surface nanoroughness of electrospun scaffolds for skeletal tissue engineering. Acta Biomater. 59, 82–93. https://doi.org/10.1016/J.ACTBIO.2017.07.003.

Darpentigny, C., Marcoux, P.R., Menneteau, M., Michel, B., Ricoul, F., Jean, B., Bras, J., Nonglaton, G., 2020. Antimicrobial cellulose nanofibril porous materials obtained by supercritical impregnation of thymol. ACS Appl. Bio. Mater 3, 2965–2975. https://doi.org/10.1021/ACSABM.0C00033/ASSET/IMAGES/LARGE/MT0C00033_0001.JPEG.

Di Salle, A., Viscusi, G., Di Cristo, F., Valentino, A., Gorrasi, G., Lamberti, E., Vittoria, V., Calarco, A., Peluso, G., 2021. Antimicrobial and antibiofilm activity of curcumin-loaded electrospun nanofibers for the prevention of the biofilm-associated infections. Molecules 26, 4866–4882. https://doi.org/10.3390/MOLECULES26164866.

Field, C.K., Kerstein, M.D., 1994. Overview of wound healing in a moist environment. Am. J. Surg. 167, S2–S6. https://doi.org/10.1016/0002-9610(94)90002-7.

Franco, P., Belvedere, R., Pessolano, E., Liparoti, S., Pantani, R., Petrella, A., Marco, I De, 2019. PCL/Mesoglycan devices obtained by supercritical foaming and impregnation. Pharmaceutics. 11, 631. https://doi.org/10.3390/PHARMACEUTICS11120631.

Franco, P., Pessolano, E., Belvedere, R., Petrella, A., De Marco, I., 2020. Supercritical impregnation of mesoglycan into calcium alginate aerogel for wound healing. J. Supercrit. Fluids 157, 104711. https://doi.org/10.1016/J.SUPFLU.2019.104711.

Fu, Y., Kao, W.J., 2010. Drug release kinetics and transport mechanisms of non-degradable and degradable polymeric delivery systems. Expert Opin. Drug Deliv. https://doi.org/10.1517/17425241003602259.

García-Casas, I., Crampon, C., Montes, A., Pereyra, C., Martínez de la Ossa, E.J., Badens, E., 2019. Supercritical CO2 impregnation of silica microparticles with quercetin. J. Supercrit. Fluids 143, 157–161. https://doi.org/10.1016/J.SUPFLU.2018.07.019.

Gurtner, G.C., Werner, S., Barrandon, Y., Longaker, M.T., 2008. Wound repair and regeneration. Nature 453 (7193), 314–321. https://doi.org/10.1038/nature07039.

Joshi, M.K., Tiwari, A.P., Pant, H.R., Shrestha, B.K., Kim, H.J., Park, C.H., Kim, C.S., 2015. In situ generation of cellulose nanocrystals in polycaprolactone nanofibers: effects on crystallinity, mechanical strength, biocompatibility, and biomimetic mineralization. ACS Appl. Mater. Interfaces 7, 19672–19683. https://doi.org/10.1021/ACSAMI.5B04682/ASSET/IMAGES/LARGE/AM-2015-04682D_0013.JPEG.

Kasi, G., Gnanasekar, S., Zhang, K., Kang, E.T., Xu, L.Q., 2022. Polyurethane-based composites with promising antibacterial properties. J. Appl. Polym. Sci. 139, 52181. https://doi.org/10.1002/APP.52181.

Kataria, K., Gupta, A., Rath, G., Mathur, R.B., Dhakate, S.R., 2014. In vivo wound healing performance of drug loaded electrospun composite nanofibers transdermal patch. Int. J. Pharm. 469, 102–110. https://doi.org/10.1016/J.IJPHARM.2014.04.047.

Korting, H.C., Schöllmann, C., White, R.J., 2011. Management of minor acute cutaneous wounds: importance of wound healing in a moist environment. J. Eur. Acad. Dermatol. Venereol. 25, 130–137. https://doi.org/10.1111/J.1468-3083.2010.03775.X.

Mircioiu, C., Voicu, V., Anuta, V., Tudose, A., Celia, C., Paolino, D., Fresta, M., Sandulovici, R., Mircioiu, I., 2019. Mathematical modeling of release kinetics from supramolecular drug delivery systems. Pharmaceutics. https://doi.org/10.3390/pharmaceutics11030140.

Mistry, P., Chhabra, R., Muke, S., Narvekar, A., Sathaye, S., Jain, R., Dandekar, P., 2021. Fabrication and characterization of starch-TPU based nanofibers for wound healing applications. Mater. Sci. Eng. C 119, 111316. https://doi.org/10.1016/J.MSEC.2020.111316.

Morales-Gonzalez, M., Arévalo-Alquichire, S., Diaz, L.E., Sans, J.Á., Vilarinõ-Feltrer, G., Gómez-Tejedor, J.A., Valero, M.F., 2020. Hydrolytic stability and biocompatibility on smooth muscle cells of polyethylene glycol–polycaprolactone-based polyurethanes. J. Mater. Res. 35, 3276–3285. https://doi.org/10.1557/JMR.2020.303.

Morales-González, M., Díaz, L.E., Dominguez-Paz, C., Valero, M.F., 2022. Insights into the design of polyurethane dressings suitable for the stages of skin wound-healing: a systematic review. Polymers (Basel) 14. https://doi.org/10.3390/POLYM14152990.

Mottola, S., Viscusi, G., Iannone, G., Belvedere, R., Petrella, A., De Marco, I., Gorrasi, G., 2023. Supercritical impregnation of mesoglycan and lactoferrin on polyurethane electrospun fibers for wound healing applications. Int. J. Mol. Sci. 24, 9269. https://doi.org/10.3390/IJMS24119269.

Novizio, N., Belvedere, R., Pessolano, E., Morello, S., Tosco, A., Campiglia, P., Filippelli, A., Petrella, A., 2021. ANXA1 contained in EVs regulates macrophage polarization in tumor microenvironment and promotes pancreatic cancer progression and metastasis. Int. J. Mol. Sci. 22, 11018. https://doi.org/10.3390/IJMS222011018.

Rezvani Ghomi, E., Khalili, S., Nouri Khorasani, S., Esmaeely Neisiany, R., Ramakrishna, S., 2019. Wound dressings: current advances and future directions. J. Appl. Polym. Sci. 136, 47738. https://doi.org/10.1002/APP.47738.

Romero, A.P., Costa, J.B., Castel-maroteaux, I., Chulia, D., 1989. Statistical optimization of a controlled release formulation obtained by a double compression process: application of an hadamard matrix and a factorial design. Drug Dev. Ind. Pharm. 15, 2419–2440. https://doi.org/10.3109/03639048909052539.

Saha, K., Dutta, K., Basu, A., Adhikari, A., Chattopadhyay, D., Sarkar, P., 2020. Controlled delivery of tetracycline hydrochloride intercalated into smectite clay using polyurethane nanofibrous membrane for wound healing application. Nano-Structures & Nano-Objects 21, 100418. https://doi.org/10.1016/J.NANOSO.2019.100418.

Thamarai Selvi, R., Prasanna, A.P.S., Niranjan, R., Kaushik, M., Devasena, T., Kumar, J., Chelliah, R., Oh, D.H., Swaminathan, S., Devanand Venkatasubbu, G., 2018. Metal oxide curcumin incorporated polymer patches for wound healing. Appl. Surf. Sci. 449, 603–609. https://doi.org/10.1016/J.APSUSC.2018.01.143.

Viscusi, G., Lamberti, E., Vittoria, V., Gorrasi, G., 2021. Coaxial electrospun membranes of poly(ε-caprolactone)/poly(lactic acid) with reverse core-shell structures loaded with curcumin as tunable drug delivery systems. Polym. Adv. Technol. 32, 4005–4013. https://doi.org/10.1002/PAT.5404.

Viscusi, G., Lamberti, E., D'Amico, F., Tammaro, L., Vigliotta, G., Gorrasi, G., 2023a. Design and characterization of polyurethane based electrospun systems modified with transition metals oxides for protective clothing applications. Appl. Surf. Sci. 617, 156563 https://doi.org/10.1016/J.APSUSC.2023.156563.

Viscusi, G., Lamberti, E., Rosaria Acocella, M., Gorrasi, G., 2023b. Production of electrospun hybrid membranes based on polyamide 6 reinforced with hemp fibers dissolved in 1-ethyl-3-methylimidazolium dicyanamide ionic liquid. J. Mol. Liq. 387, 122656 https://doi.org/10.1016/J.MOLLIQ.2023.122656.

Viscusi, G., Paolella, G., Lamberti, E., Caputo, I., Gorrasi, G., 2023c. Quercetin-loaded polycaprolactone-polyvinylpyrrolidone electrospun membranes for health application: design, characterization modeling and cytotoxicity studies. Membranes 13, 242. https://doi.org/10.3390/MEMBRANES13020242.

Wang, C., Wang, J., Zeng, L., Qiao, Z., Liu, X., Liu, H., Zhang, J., Ding, J., 2019. Fabrication of electrospun polymer nanofibers with diverse morphologies. Molecules 24, 834. https://doi.org/10.3390/MOLECULES24050834.

Weibull, W., 1951. A statistical distribution function of wide applicability. JAM 18, 293–297.

Yao, X., Bunt, C., Cornish, J., Quek, S.Y., Wen, J., 2013. Improved RP-HPLC method for determination of bovine lactoferrin and its proteolytic degradation in simulated gastrointestinal fluids. Biomed. Chromatogr. 27, 197–202. https://doi.org/10.1002/BMC.2771.

Yuan, H., Chen, L., Hong, F.F., 2021. Homogeneous and efficient production of a bacterial nanocellulose-lactoferrin-collagen composite under an electric field as a matrix to promote wound healing. Biomater. Sci. 9, 930–941. https://doi.org/10.1039/D0BM01553A.